Jurnal Elektronika dan Telekomunikasi (JET), Vol. 20, No. 2, December 2020, pp. 82-88
Accredited by RISTEKDIKTI, Decree No: **32a/E/KPT/2017**
doi: 10.14203/jet.v20.82-88

Thermopower Enhancement of Rutile-type SnO_2 Nanocrystalline Using Facile Co-Precipitation Method

Nadya Larasati Kartika [a,*], Budi Adiperdana [b], Asep Ridwan Nugraha [a], Ardita Septiani [a], Dadang Mulyadi [a], Pepen Sumpena [a], Asep Rusmana [a], Dedi [a]

[a] *Research Center for Electronics and Telecommunication*
Indonesian Institute of Sciences
Kampus LIPI, Jl. Sangkuriang Building 20, 4th Floor
Bandung, Indonesia
[b] *Department of Physics, Faculty of Mathematics and Sciences*
Universitas Padjadjaran
Sumedang, Indonesia

Abstract

Metal oxide semiconductor has attracted so much attention due to its high carrier mobility. Herein, thermoelectric study of nanocrystalline SnO_2 through a simple co-precipitation method is conducted to enhance the Seebeck coefficient (*S*). X-ray diffraction, thermogravimetric analysis (TGA), resistivity (ρ), Seebeck coefficient (*S*), and power factor (PF) measurements are conducted to analyze the thermoelectric properties of the material. The measurements show that there are two interesting results, which are the unusual resistivity behavior and the high value of the *S*. Resistivity behavior shows a non-reflective intermediate semiconductor-metals behavior where the turning point occurs at 250 ºC. This behavior is strongly correlated to the surface oxide reaction due to annealing temperature. The maximum *S* likely occurs at 250 ºC, since the curve shows a slight thermopower peak at 250 ºC. The value of the *S* is quite high with around twenty times higher than other publications about SnO_2 thermoelectric material, this happens due to the bandgap broadening. The energy gap of SnO_2 calculated using density functional theory (DFT), which was performed by Quantum Espresso 6.6. The result shows that there is a broadening energy gap at different momentum or wave factor. Nanocrystalline semiconductors material is giving an impact to increase the width of bandgap due to quantum confinement and could enhance the thermopower especially in SnO_2 nanocrystalline.

Keywords: nanocrystalline, metal-oxide, thermoelectric, tin-dioxide, Seebeck, co-precipitation.

I. INTRODUCTION

Thermoelectric materials are promising candidates as harvesting energy devices for converting waste heat into electricity [1]. Thermoelectric could be applied as solid-state refrigerators or heat pumps. One advantage of thermoelectric is it does not use any moving parts and environmentally harmful fluids. Due to their high reliability and simplicity, thermoelectric materials are used extensively in fields such as space power generation and a variety of cooling applications [2]. Thermoelectric performance is determined by the dimensionless figure of merit (*ZT*) [2], [3], which is denoted by (1).

$$ZT = \frac{S^2 \sigma T}{\kappa} \quad (1)$$

where *S* is Seebeck coefficient representing a significant temperature difference which is required to generate electrical energy, σ is electrical conductivity, κ is thermal conductivity, and *T* is the absolute temperature. In order to increase thermoelectric material performance, elevating the optimization of the *ZT* value is required. To maximize *ZT* value, the *S*, large σ, and low κ are needed simultaneously. However, there are conflicting parameters in optimizing *ZT*, since the *S*, σ, and κ_e are strongly coupled by carrier concentration (*n*), and difficult to control those variables independently following Wiedemann-Franz Law [4], [5].

Based on (1), to achieve a high *ZT* value, the enhancement of the *S* is needed. There are two conventional strategies to optimize the *ZT* values, which are: (1) enhancing the power factor (PF) by point defect engineering, and band engineering; (2) independently reducing the lattice thermal conductivity (κ_L) by structural nano-crystallization, interface engineering, and hierarchical architecting, or designing novel thermoelectric materials with intrinsically low κ [6], [7].

A semiconductor material is a good candidate as a thermoelectric application since it can be doped to achieve a single n-type or p-type carrier for enhancing the *S*. A mixture of n-type and the p-type carrier will lead to lowering the *S* [8]. In other words, both low *n* and high *n* of semiconductor behavior can obtain large *S*.

Several material types attracted so much attention in the thermoelectric application, such as chalcogenide metals [9], SiGe alloy [10], [11], silicon based thermoelectric materials [12], and skutterudites [13]. There are several thermoelectric materials commercially provided from low to high temperature, which are Bi_2Te_3 (300–500 K) [14], PbTe (500–600 K) [15], and SiGe (600–800 K) [11]. The progress of thermoelectric material is still limited for practical application since

* Corresponding Author.
Email: nadya.larasati.kartika@lipi.go.id
Received: October 14, 2020 ; Revised: November 25, 2020
Accepted: December 10, 2020 ; Published: December 31, 2020

their applications are largely restricted by the toxicity, limited element resources, and material degradation at high temperatures because of the temperature limitation due to phase transformation at high temperatures [2], [16].

Metal oxide-based material is one of the candidates for thermoelectric application, since it has low-mobility materials properties, primarily because of its highly ionic characters, abundance in nature, and non-toxicity [16], [17]. However, the lower mobility in metal oxide thermoelectric leads to larger lattice thermal conductivity and thus, it is quite difficult to achieve high *ZT* [5].

Tin-dioxide is one of the metal-oxide group that is a candidate of an n-type semiconductor material due to its electrical conductivity simultaneously with optical properties and high-temperature stability [18], [19]. SnO_2 has a wide-bandgap (3.6 eV) and the value of bandgap width is a fundamental property in semiconductor material [8], [20] to achieve desired properties such as elevating the *S* to enhance the *ZT*. Fonstad *et al.* reported the Hall mobility (μ_h) value of SnO_2 single-crystal was one-order larger than the drift mobility (μ_d) of copper [21].

SnO_2 as thermoelectric material has been synthesized using several techniques and showed a nearly similar *S* coefficient value. Ferreira et al did SnO_2 n-type thermoelectric thin-film synthesis by radio frequency (rf) sputtering and showed *S* of -225 μV/K, ρ below 10^{-3} Ω.m, and around 10^{-4} W/m.K² for PF [22]. Bagheri et al also did SnO_2 thin films synthesis using spray pyrolysis technique and showed n-type thermoelectric. The *S* effect showed -255 μV/K with n-type thermoelectric material and resistivity 1.3 x 10^{-2} Ω.cm [23]. SnO_2 has been synthesized using a solid-state method by Paulson et al [18]. The results showed the *S* was between -220 and -230 μV/K, the crystallite size was 83.6 nm, and the PF was between 6 and 7 x 10^{-6} W/m.K². However, the PF of each result showed big different values due to the σ for each material could be different due to the size of the bandgap. The limiting point of SnO_2 as a thermoelectric application was low thermoelectric performance due to large thermal conductivity around 40 $Wm^{-1}K^{-1}$. Kerrami *et al.* published a simulation about enhanced *ZT* of SnO_2 by modulating the energy band structure through an applied strain [19].

In order to enhance the *S* coefficient, nanostructured materials are required. Nanostructured material often shows different properties with the bulk material due to strong surface interactions between closely packed nanoparticles, a large surface to volume ratio, and quantum confinement effects due to the tiny size. Decreasing particle size will reduce the κ and preserve *n* due to confining electron motion into a specified energy level. The electron motion confinement makes discreteness of level energy and widens up the bandgap. Increasing the bandgap width generating enhancement of the *S* and could elevate the effectiveness of PF of thermoelectric material [8], [20], [24].

This paper aims to characterize the thermoelectric properties of undoped SnO_2 nanocrystalline. The co-precipitation method is used as a synthesis method to obtain nanocrystalline materials to increase the bandgap width to enhancing the *S*. This method used since the published papers about the synthesis SnO_2 co-precipitation method are rare to find because of the majority used for gas sensing and photovoltaic application. The method is commonly used to synthesized nanocrystalline materials [25]. Moreover, the co-precipitation method is facile, low energy, and practicable in reproducibility.

II. EXPERIMENTAL SECTION

A. Materials

$SnCl_2.2H_2O$ (Merck) and ammonia (Merck) were used as starting materials with a concentration of 0.22 M and 2 M, respectively, using deionized (DI) water as a solution to synthesize SnO_2 powder using a simple co-precipitation method. A magnetic stirrer with a hot plate was equipped to dissolve the $SnCl_2.2H_2O$ in DI water at low-speed stirring under ambient temperature. The temperature of the solution was increased to 40 °C while the ammonia slowly dropped into the solution until the pH reached 10 - 11. Then the temperature was raised to 90 °C and the solution was stirred for 2 h.

The solution was let cool down to room temperature, then the precipitation was collected and cleaned for several times using DI water. The white powder was dried at 60 °C for 24 h and annealed at 800 °C for 2 h under ambient pressure.

B. Characterization

The phase of powder SnO_2 was determined by using Bruker D8-Advance X-ray powder diffractometer with 0.02 angle steps between 20º to 90º of 2θ using Cu Kα radiation. The results were then refined using Rietveld analysis to obtain the lattice and structure parameter. The crystallite size and strain were calculated manually in python from the X-ray diffraction (XRD) pattern perspective using the Williamson-Hall (W-H) plot method [26], [27]. Grain size, morphology, and elemental composition of SnO_2 were determined using a scanning electron microscope with an energy dispersive X-ray spectroscopy (SEM/EDS) JEOL-JSM IT 300.

Thermoelectric properties of SnO_2 were examined using Linseis LSR-4 in the range of 150 to 450 ºC of temperature. That range was obtained from thermogravimetry analysis (TGA) characterization using NETZSCH TG 209 F1 Libra TGA209F1E-00 with the heat rate 10º/min in the range 30 - 600 ºC under an oxygen atmosphere. The band structure of SnO_2 nanocrystalline was analyzed using theoretical calculation using Density Functional Theory (DFT) method and performed by Quantum Espresso 6.6.

III. RESULTS AND DISCUSSIONS

X-ray powder diffraction pattern of SnO_2 is shown in Figure 1, where all the peaks belong to SnO_2 structure with space group P42/m n m and there is no peak belonging to other elements indexed to the Powder Diffraction File (PDF) cassiterite tetragonal SnO_2 (PDF-96-900-7434) [28]. The refinement was done using the Rietveld method [29] and obtained 1.6, 2.46, 8.61, and 5.49 for the Goodness of Fitting (GoF) index; Chi^2, Rwp, and Rf, respectively.

The crystallography structure is shown in Figure 2. The Sn-atom is surrounded by six oxygens and resulted in rutile phasethat has a tetragonal crystal structure. All refined parameters are shown in Table 1.

The peak broadening from X-Ray powder diffraction is attributed by the crystallite size and microstrain, which represents the displacement of atoms from their original positions and instrumental broadening. Indirect crystallite size and microstrain determination could be done using the XRD pattern perspective. The Williamson-Hall (W-H) plot is used since the Scherrer equation gives a rough estimation of a crystallite size where the line broadening is only from crystallite size contribution and neglecting other parameters i.e. strain, instrumental broadening, preferred orientation, and shape factor. The small crystallite size is causing the crystal growth limitation and change to imperfect crystal, which leads to broadening in the diffraction peak [26]. Williamson-Hall (W-H) plot is a technique to separate the contributions of crystallite size and microstrain to the peak broadening in X-Ray powder diffraction patterns with Lorentzian profiles, which is denoted by (2) [27].

$$\beta = \beta_D + \beta_\epsilon \quad (2)$$

TABLE 1
CRYSTAL DATA AND REFINEMENT RESULT FROM SnO_2

Structure Parameter					
Atom	**x**	**y**	**z**	**Uc**	**Site**
Sn	0.00000	0.00000	0.00000	1.000	2a
O	0.30350	0.30350	0.00000	1.043	4f
Lattice Parameter					
a	**b**	**c**	**α**	**β**	**γ**
4.7377 Å	4.7377 Å	3.1864 Å	90°	90 °	90 °

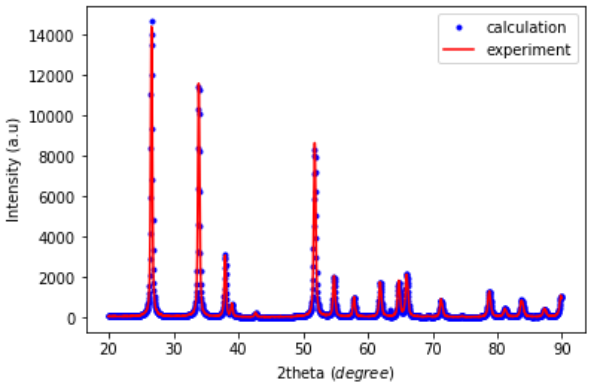

Figure 1. X-ray Diffraction Refinement.

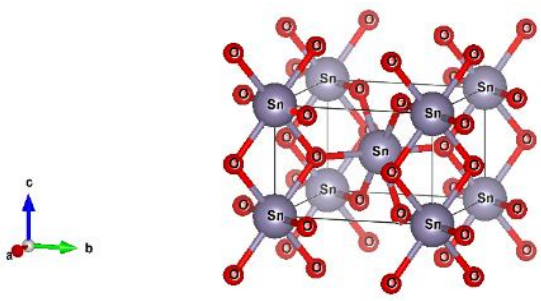

Figure 2. Structure of Rutile SnO_2.

Scherrer equation is described in (3).

$$\beta_D = \frac{k\lambda}{D cos\theta} \quad (3)$$

where β_D is Full Width Half at Maximum (FWHM) in radians, k is the shape factor, D is the crystallite size, θ is the peak position in radians, and λ is the wavelength of the X-ray source. Peak broadening contribution from micro-strain is given by (4).

$$\beta_\epsilon = 4\epsilon\, tan\theta \quad (4)$$

where β_ϵ is the FWHM due to strain and ε is the strain. The Williamson-Hall equation can be written as (5).

$$\beta cos\theta = \epsilon(4\, sin\theta) + \frac{k\lambda}{D} \quad (5)$$

Compared to the linear fitting equation, microstrain value and crystallite size were obtained from the slope and intercept, respectively. The result is shown in Figure 3. The slope was obtained as micro-strain in negative value indicates that there is lattice compression [30] with -0.00033 occurrence. Then, the crystallite size from the W-H plot is around 70 nm.

The morphology of SnO_2 was analyzed by SEM and the result in Figure 4(a) shows that the material most likely has a near-spherical shape that tends to oval shape. Other publications about co-precipitation SnO_2 synthesis method showed a similar shape [31]–[33].

The grain size distribution was determined from the micrograph and the result is shown in Figure 4(b), giving an average grain size of around 71 nm. The results from the SEM is used to compare the crystallite size from the approximation based on the real morphology of SnO_2 material to that obtained from the W-H plot. Both methods give almost similar value. The results from the W-H plot method and SEM examination are summarized in Table 2.

TABLE 2
WIILIAMSON-HALL PLOT DATA RESULT

Sample	Strain	Crystallite Size (nm)	Grain Size from SEM (nm)
SnO_2	-0.00033	70	71.1

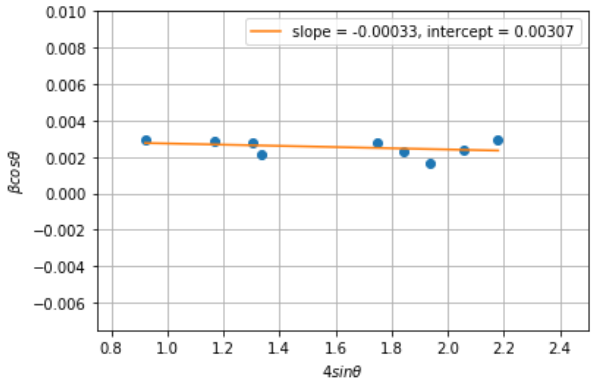

Figure 3. Williamson-Hall Plot from SnO_2.

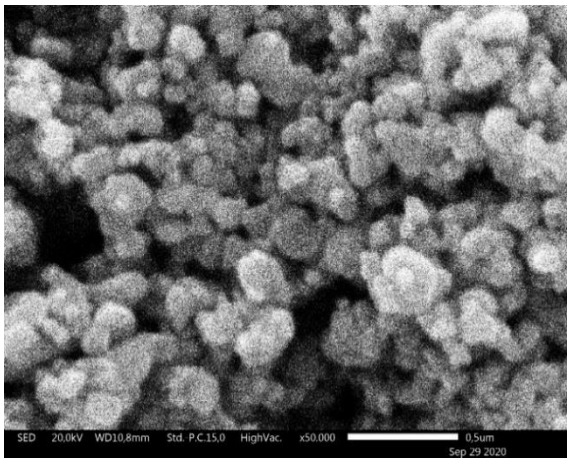

(a)

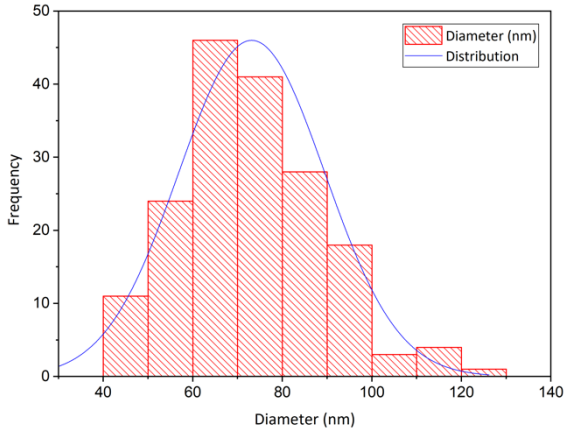

(b)

Figure 4. (a). SEM Image of SnO_2 Nanocrystalline (b). Histogram and Distribution Curve of the Grain Size Diameter of SnO_2 Nanocrystals (in nm).

The temperature range of SnO_2 thermoelectric properties is determined by TGA measurement to observe the decomposition of the sample based on the temperature, so that heat induced sample loss could be avoided during thermoelectric measurement. Figure 5 shows the TGA result and its differential curve.

The decreasing peak on the differential curve at 36.1 ºC possibly indicated the evaporation of some solvents. As shown in Table 3, the changing mass of the sample occurred at four temperature ranges. Overall, the curve shows that the sample undergoes multistage decomposition progress, however, there is an uncommon increasing weight at 113.2 - 286.3 ºC due to oxidation [34], [35] since the measurement was conducted under oxygen atmosphere [29], [30]. After being transformed into metal oxide material, as the temperature increases, the material attracts electrons from oxygen which leads to increased weight due to surface oxide reaction. Then, the weight of SnO_2 decreased slowly after 600 ºC [36].

The electrical resistivity curve in Figure 6(a) shows two-phase of conductivity behavior. As the temperature increases, charge carriers were thermally activated, which increased their drift mobility (μ_d) and decreased ρ from 150 – 260 ºC. This shows a typical semiconductor behavior. Then, the ρ started to increase from 250 ºC, which indicates conductivity from the characteristic of metal. From the curve, it could be said that the character of SnO_2 conductivity exhibits non-reflective intermediate properties between semiconductor and metal.

This notable change could be strongly related to the TGA curve which has a slight increase in weight percentage around 113.2 - 286.3 ºC, while temperature increases after 113.2 - 286.3 ºC range, the oxygen seems to be excited at a higher temperature and the SnO_2 tends to have metal resistivity behavior. These properties are also found in CuO_2 [37] due to annealing temperature and the material phases formed are calculated using Lichtenecker's formula for resistivity of two-phase alloys.

The *S* curve is shown in Figure 6(b), the negative sign indicates that SnO_2 nanocrystalline is an n-type semiconductor. The *S* is approximately ten times higher than any other publication about SnO_2. This is caused by the *S* in semiconductor will be much larger than it is in metals due to the presence of a bandgap which breaks the symmetry between electron and hole [38]. The *S* curve did not show a clear thermopower peak, but the point at 250 ºC is noteworthy, which shows -5.79 x 10^3 μV/K.

TABLE 3
MASS CHANGE PERCENT FROM TGA MEASUREMENT RESULT

Mass Change (%)	Temperature Range (ºC)	
	Min	Max
-0.32	26.4	112.7
0.18	112.7	286.0
-0.07	286.0	362.5
-0.76	362.5	599.9

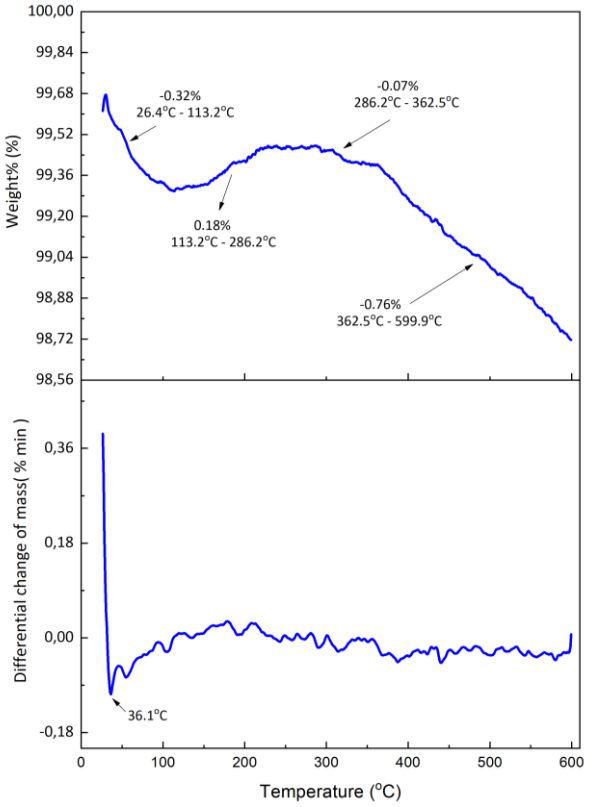

Figure 5. TGA Diagram and Differential Curve from TGA Diagram of SnO_2 Nanocrystalline.

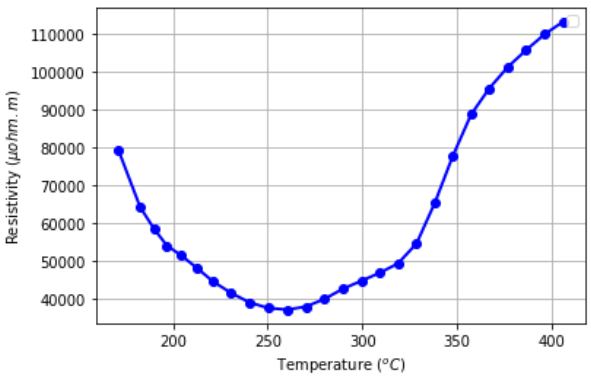

(a)

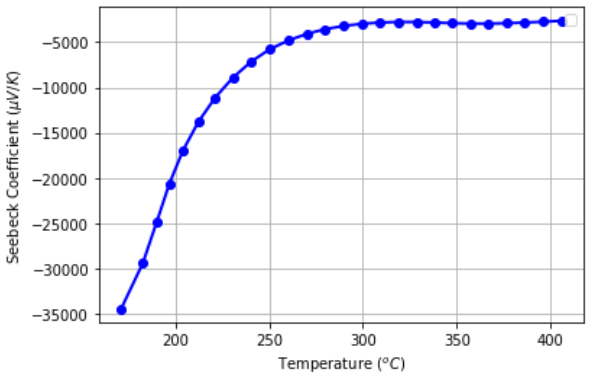

(b)

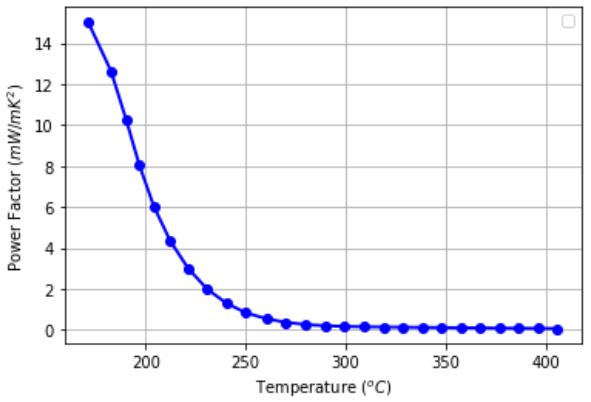

(c)

Figure 6. Thermoelectric Properties Result (a) Resistivity (b) Absolute Seebeck Coefficient, and (c) Power Factor.

The absolute *S* at temperature (T) < 250 °C drops significantly followed by conductivity as well, this is typically semiconductor behavior since the Fermi level is moving into the valence band [38]. The *S* at T > 250 °C, the curve decreases slowly and shows metals behavior due to increasing conductivity.

The relation between the energy gap and the *S* in a semiconductor. Goldsmid and Sharp developed an analytical expression on the bandgap and the maximum Seebeck coefficient through Goldsmid-Sharp in (6) [24], [39].

$$E_g = 2e|S|_{max}T_{max} \quad (6)$$

where E_g is the energy gap, $|S|_{max}$ is Seebeck coefficient maximum, and T_{max} is the temperature where the *S* maximum occurs. Goldsmid-Sharp is a useful tool for estimating the energy gap through temperature dependence *S* measurement value [24].

Theoretical computation of band structure is employed as an explanation about the broadening band gap which occurs in SnO_2 nanocrystalline using density functional theory (DFT). The gap energy of material has different values for each wave factor or momentum, hence, all the Brillouin Zone (BZ) should be included in reciprocal space. To determine the energy gap and correct the charge-charge and spin-spin interaction, an exchange-correlation function is needed. There are a lot of exchange-correlation function types and the property is unique for each material structure.

In this paper, a band structure and density of state (DOS) were performed using Quantum Espresso 6.6 [40] with Projector Augmented Wave (PAW) [41] and Perdew-Burke-Emzerhof for solids (PBEsol) exchange-correlation which is generally used to determine the energy gap [42]. Band structure and DOS are calculated using lattice constant from the experiment result and compared with the optimized structure to represent the bulk structure (a = 4.7690, c=3.2295).

The PBEsol exchange-correlation method is used to explain the gap energy broadening phenomena, however, to obtain the gap energy near to the exact value needs another exchange-correlation method which is more complex than PBEsol [43]. In this paper, the use of the PBEsol exchange-correlation method is proper enough to explain the broadening of the energy gap phenomena. The calculation result is shown in Figure 7, the energy gap minimum at Γ position has 1.114 eV from the experiment structure and 0.781 eV from the optimized structure, and all energy gap calculation results at each position are summarized in Table 4.

TABLE 4
ENERGY GAP RESULT FOR EACH POSITION

Position	Energy Gap (eV)	
	SnO_2 Optimized Structure	SnO_2 nanocrystalline
Γ	0.781	1.110
X	4.310	4.614
M	4.852	5.204
Z	6.504	6.866
R	6.273	6.581
A	4.921	5.233

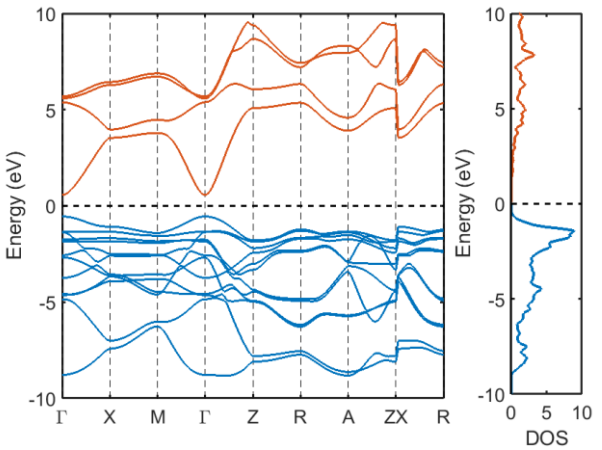

Figure 7. Band Structure and DOS of SnO_2 Nanocrystalline Calculation using DFT.

TABLE 5
LATTICE PARAMETER COMPARISON BETWEEN OPTIMIZED STRUCTURE (BULK) AND NANOCRYSTALLINE STRUCTURE

Lattice Parameter	SnO_2 Optimized Structure	SnO_2 nanocrystalline
a	4.7690 Å	4.7364 Å
b	4.7690 Å	4.7364 Å
c	3.2295 Å	3.1857 Å

It can be clearly seen that the SnO_2 nanocrystalline shows a broadening of the energy gap at each position. This result is in good agreement with Zhou *et al*. publication which exhibits a similar result with this paper for energy gap broadening compared to the optimized structure and the experiment structure at Γ position [44]. The broadening value of the energy gap from the experiment at Γ position occurs due to lattice compression [44] which is shown in Table 5. The lattice compression is also exhibited in the W-H plot calculation and shows a negative strain value due to decreasing crystalline size [30], [45].

The nanocrystalline structure in SnO_2 semiconductor has most likely gave an impact to the increase in the width of the bandgap due to quantum confinement and the effect of the internal strain. The nanostructuring makes the particle too small to be comparable with the wavelength of the electron, the motion of the electron is restricted to the specified energy through quantum confinement.

The confinement of moving electrons is making the valence and conduction band split and discrete due to restricted the electron movement into specified energy, which results in widening up the bandgap [8], [20], [46]. Sahana *et al*. [20] increased the SnO_2 bandgap from 3.89 to 4.5 eV through nanostructuring by a controlled choice of composition and annealing temperature. The enhancement of thermopower due to quantum confinement is also giving an impact on lowering the κ [8], [47].

Figure 6(c) shows SnO_2 reaches the maximum PF at 171 ^oC with the value of 15.03 x 10^{-2} W/m.K^2. This value is much related to the *S* and σ. When the temperature is rising, the charge carrier conductivity also increases.

Nonetheless, the high *S* value cannot meet the clarity yet since many things could affect the materials. However, the strong one which is correlated to the enhancement of the *S* is the bandgap of the materials with temperature influences. Both resistivity behavior and the interesting *S* in SnO_2 nanocrystalline need further investigation using a comprehensive bandgap measurement and theoretical approach relating to the oxygen occupancy and the temperature influence to the bandgap modification.

CONCLUSION

In summary, nanocrystalline SnO_2 was synthesized using the facile co-precipitation method. The thermoelectric properties were examined and showing two interesting results, which are the electrical resistivity (ρ) behavior to the increasing temperature due to surface oxide reaction and the high Seebeck coefficient (*S*) around twenty times higher than other publications. The relationship between the *S* and nanostructuring is strongly correlated to the bandgap broadening due to the quantum confinement process. However, those arguments need further investigation by energy gap characterization and a comprehensive theoretical approach.

ACKNOWLEDGMENT

This study has been supported by Research Center for Electronics and Telecommunications-LIPI and Research Unit for Clean Technology-LIPI for the measurement and characterization facilities.

REFERENCES

[1] Y. Yin, B. Tudu, and A. Tiwari, "Recent advances in oxide thermoelectric materials and modules," *Vacuum*, vol. 146, pp. 356–374, 2017.

[2] A. J. Minnich, M. S. Dresselhaus, Z. F. Ren, and G. Chen, "Bulk nanostructured thermoelectric materials: Current research and future prospects," *Energy Environ. Sci.*, vol. 2, no. 5, pp. 466–479, 2009.

[3] G. S. Nolas, J. Sharp, and J. Goldsmid, *Thermoelectrics: Basic Principles and New Materials Developments*. New York: Springer-Verlag Berlin Heidelberg, 2013.

[4] B. Poudel *et al.*, "High-thermoelectric performance of nanostructured bismuth antimony telluride bulk alloys," *Sci.*, vol. 320, no. 1996, pp. 634–638, 2008.

[5] S. A. Miller *et al.*, "SnO as a potential oxide thermoelectric candidate," *J. Mater. Chem. C*, vol. 5, no. 34, pp. 8854–8861, 2017.

[6] C. Li, F. Jiang, C. Liu, P. Liu, and J. Xu, "Present and future thermoelectric materials toward wearable energy harvesting," *Appl. Mater. Today*, vol. 15, pp. 543–557, 2019.

[7] Y. Zheng *et al.*, "Designing hybrid architectures for advanced thermoelectric materials," *Mater. Chem. Front.*, vol. 1, no. 12, pp. 2457–2473, 2017.

[8] Z. G. Chen, G. Hana, L. Yanga, L. Cheng, and J. Zou, "Nanostructured thermoelectric materials: Current research and future challenge," *Prog. Nat. Sci. Mater. Int.*, vol. 22, no. 6, pp. 535–549, 2012.

[9] J. F. Nakahara, T. Takeshita, M. J. Tschetter, B. J. Beaudry, and K. A. Gschneidner, "Thermoelectric properties of lanthanum sulfide with Sm, Eu, and Yb additives," *J. Appl. Phys.*, vol. 63, no. 7, pp. 2331–2336, 1988.

[10] C. M. Bhandari and D. M. Rowe, "Silicon-germanium alloys as high-temperature thermoelectric materials," *Contemp. Phys.*, vol. 21, no. 3, pp. 219–242, 1980.

[11] D. M. Rowe and V. S. Shukla, "The effect of phonon-grain boundary scattering on the lattice thermal conductivity and thermoelectric conversion efficiency of heavily doped fine-grained, hot-pressed silicon germanium alloy," *J. Appl. Phys.*, vol. 52, no. 12, pp. 7421–7426, 1981.

[12] S. at Tanusilp and K. Kurosaki, "Si-based materials for thermoelectric applications," *Mater. (Basel).*, vol. 12, no. 12, 2019.

[13] B. C. Sales, D. Mandrus, and R. K. Williams, "Filled skutterudite antimonides: A new class of thermoelectric materials," *Science*, vol. 272, no. 5266, pp. 1325–1328, 1996.

[14] B. M. S. Dresselhaus *et al.*, "New directions for low-dimensional thermoelectric materials," *Adv. Mater.*, vol. 19, pp. 1043–1053, 2007.

[15] Y. Takagiwa, Y. Pei, G. Pomrehn, and G. J. Snyder, "Dopants effect on the band structure of PbTe thermoelectric material," *Appl. Phys. Lett.*, vol. 101, no. 9, pp. 1–4, 2012.

[16] N. Okinaka and T. Akiyama, "Thermoelectric properties of nonstoichiometric TiO as a promising oxide material for high-temperature thermoelectric conversion," in *24th Int. Conf. Thermoelectr.*, USA, 2005, pp. 34–37.

[17] Y. Feng *et al.*, "Metal oxides for thermoelectric power generation and beyond," *Adv. Compos. Hybrid Mater.*, vol. 1, no. 1, pp. 114–126, 2018.

[18] A. Paulson, N. A. M. Sabeer, and P. P. Pradyumnan, "Enhanced thermoelectric property of oxygen deficient nickel doped SnO_2 for high temperature application," *Mater. Res. Express*, vol. 5, no. 4, pp. 1–21, 2018.

[19] Z. Kerrami, A. Sibari, O. Mounkachi, A. Benyoussef, and M.

Benaissa, "SnO_2 improved thermoelectric properties under compressive strain," *Comput. Condens. Matter*, vol. 18, 2019.
[20] M. B. Sahana, C. Sudakar, A. Dixit, J. S. Thakur, R. Naik, and V. M. Naik, "Quantum confinement effects and band gap engineering of SnO_2 nanocrystals in a MgO matrix," *Acta Mater.*, vol. 60, no. 3, pp. 1072–1078, 2012.
[21] C. G. Fonstad and R. H. Rediker, "Electrical properties of high-quality stannic oxide crystals," *J. Appl. Phys.*, vol. 42, no. 7, pp. 2911–2918, 1971.
[22] M. Ferreira, J. Loureiro, A. Nogueira, A. Rodrigues, R. Martins, and I. Ferreira, "SnO_2 thin film oxides produced by rf sputtering for transparent thermoelectric devices," *Mater. Today Proc.*, vol. 2, no. 2, pp. 647–653, 2015.
[23] M. M. Bagheri-Mohagheghi, N. Shahtahmasebi, M. R. Alinejad, A. Youssefi, and M. Shokooh-Saremi, "Fe-doped SnO_2 transparent semi-conducting thin films deposited by spray pyrolysis technique: Thermoelectric and p-type conductivity properties," *Solid State Sci.*, vol. 11, no. 1, pp. 233–239, 2009.
[24] Z. M. Gibbs *et al.*, "Band gap estimation from temperature dependent Seebeck measurement - Deviations from the $2e|S|_{max}T_{max}$ relation," *Appl. Phys. Lett.*, vol. 106, pp. 022112-1-022112–5, 2015.
[25] A. Rajaeiyan and M. M. Bagheri-Mohagheghi, "Comparison of sol-gel and co-precipitation methods on the structural properties and phase transformation of γ and α-Al_2O_3 nanoparticles," *Adv. Manuf.*, vol. 1, no. 2, pp. 176–182, 2013.
[26] V. D. Mote, Y. Purushotham, and B. N. Dole, "Williamson-Hall analysis in estimation of lattice strain in nanometer-sized ZnO particles," *J. Theor. Appl. Phys.*, vol. 6, pp. 1–8, 2012.
[27] G. K. Williamson and W. H. Hall, "X-Ray broadening from filed aluminium and wolfram," *Acta Metall.*, vol. 1, pp. 22–31, 1953.
[28] W. H. Baur, "*Über die Verfeinerung der Kristallstrukturbestimmung einiger Vertreter des Rutiltyps*: TiO_2, SnO_2, GeO_2 *und* MgF_2," *Acta Crystallogr.*, vol. 9, no. 6, pp. 515–520, 1956.
[29] L. B. McCusker, R. B. Dreele, D. E. Cox, D. Louer, and P. Scardi, "Rietveld refinement guidelines," *J. Apply. Cryst.*, vol. 32, pp. 36–50, 1999.
[30] N. S. Gonçalves, J. A. Carvalho, Z. M. Lima, and J. M. Sasaki, "Size-strain study of NiO nanoparticles by X-ray powder diffraction line broadening," *Mater. Lett.*, vol. 72, pp. 36–38, 2012.
[31] M. Aziz, S. S. Abbas, and W. R. W. Baharom, "Size-controlled synthesis of SnO_2 nanoparticles by sol-gel method," *Mater. Lett.*, vol. 91, pp. 31–34, 2013.
[32] V. Kumar *et al.*, "Effect of solvent on crystallographic, morphological and optical properties of SnO_2 nanoparticles," *Mater. Res. Bull.*, vol. 85, pp. 202–208, 2017.
[33] H. Uchiyama, H. Ohgi, and H. Imai, "Selective preparation of SnO_2 and SnO crystals with controlled morphologies in an aqueous solution system," *Cryst. Growth Des.*, vol. 6, no. 9, pp. 2186–2190, 2006.
[34] S. Loganathan, R. B. Valapa, R. K. Mishra, G. Pugazhenthi, and S. Thomas, "Thermogravimetric analysis for characterization of nanomaterials," in *Thermal and Rheological Measurement Techniques for Nanomaterials Characterization*, vol. 3., Netherlands: Elsevier Inc., 2017.
[35] *Interpreting TGA curves: information for users of Mettler Toledo thermal analysis systems*," Mettler Toledo, 2001, pp. 1–20.
[36] J. Huang, N. Matsunaga, K. Shimanoe, N. Yamazoe, and T. Kunitake, "Nanotubular SnO_2 templated by cellulose fibers: Synthesis and gas sensing," *Chem. Mater.*, vol. 17, no. 13, pp. 3513–3518, 2005.
[37] V. Nadutov, A. Perekos, V. Kokorin, S. Konoplyuk, and T. Kabantsev, "Influence of oxidation on electrical properties of compacted Cu nanopowders," *Nanoscale Res. Lett.*, vol. 11, pp. 1-4, 2016.
[38] M. Markov, S. E. Rezaei, S. N. Sadeghi, K. Esfarjani, and M. Zebarjadi, "Thermoelectric properties of semimetals," *Phys. Rev. Mater.*, vol. 3, no. 9, pp. 1–7, 2019.
[39] H. J. Goldsmid and J. W. Sharp, "Estimation of the thermal band gap of a semiconductor from Seebeck measurements," *J. Electron. Mater.*, vol. 28, no. 7, pp. 869–872, 1999.
[40] P. Giannozi *et al.*, "Advanced capabilities for materials modelling with Quantum ESPRESSO," *J. Phys. Condens. Matter*, vol. 29, no. 46, pp. 1–30, 2017.
[41] P. E. Blöchl, "Projector augmented-wave method," *Phys. Rev. B*, vol. 50, no. 24, pp. 17953–17979, 1994.
[42] J. P. Perdew *et al.*, "Restoring the density-gradient expansion for exchange in solids and surfaces," *Phys. Rev. Lett.*, vol. 100, no. 13, pp. 1–4, 2008.
[43] Á. Morales-García, R. Valero, and F. Illas, "An empirical, yet practical way to predict the band gap in solids by using density functional band structure calculations," *J. Phys. Chem. C*, vol. 121, no. 34, pp. 18862–18866, 2017.
[44] W. Zhou, Y. Liu, Y. Yang, and P. Wu, "Band gap engineering of SnO_2 by epitaxial strain: Experimental and theoretical investigations," *J. Phys. Chem. C*, vol. 118, pp. 6448–6453, 2014.
[45] Y. Zhao and J. Zhang, "Microstrain and grain-size analysis from diffraction peak width and graphical derivation of high-pressure thermomechanics," *J. Appl. Cryst.*, vol. 41, no. 6, pp. 1095–1108, 2008.
[46] M. B. Sahana *et al.*, "Bandgap engineering by tuning particle size and crystallinity of SnO_2 - Fe_2O_3 nanocrystalline composite thin films," *Appl. Phys. Lett.*, vol. 93, no. 23, pp. 2–5, 2008.
[47] S. Hao, V. P. Dravid, M. G. Kanatzidis, and C. Wolverton, "Computational strategies for design and discovery of nanostructured thermoelectrics," *Nature Partner J. Comput. Mater.*, vol. 5, pp. 1–10, 2019.